Article

Bi-Photon Entangled Airy Beams through Unstable Oceanic Turbulence

Donghui Yang [1], Zhou Yu [1], Zhengda Hu [1,2,3], Wenhai Wang [1] and Yun Zhu [1,2,3,*]

1   School of Science, Jiangnan University, Wuxi 214122, China
2   Jiangsu Provincial Research Center of Light Industrial Optoelectronic Engineering and Technology, Wuxi 214122, China
3   Key Laboratory of Quantum Information, University of Science and Technology of China, Chinese Academy of Sciences, Hefei 230026, China
*   Correspondence: yunzhu99@jiangnan.edu.cn

Abstract: Orbital angular momentum (OAM) carried by bi-photon entangled Airy beams in unstable oceanic turbulence is theoretically investigated. The analytical expression of the spatial coherence radius of a spherical wave in the unstable stratification oceanic turbulence is derived to obtain the relative detection probability of bi-photon entangled Airy beams. The relative detection probability of OAM carried by bi-photon entangled Airy beams acquires significant enhancements—up to 62% compared to the same measurement for the single photon system over a distance of 100 m. Lower-order bi-photon entangled Airy beams with larger wavelengths, and main ring radius are less affected by oceanic turbulence. A larger main ring radius also contributes to reducing the fluctuations in detection probability. Oceanic turbulence dominated by salinity fluctuations induces more adverse effects on the OAM, as well as a stronger strength of the turbulence.

Keywords: Airy beams; bi-photon entanglement; orbital angular momentum; oceanic turbulence

1. Introduction

Underwater optical communication (UOC) based on orbital angular momentum (OAM) has a high capacity due to the arbitrary base-N quantum digits [1–3], while oceanic turbulence in the propagation would seriously distort the helical phase structure of OAM [4], giving rise to degradation of the UOC system. Spatial power spectrum as a statistical method can describe this kind of optical turbulence [5–7]. Nikishov proposed an oceanic spectrum based on the common assumption that the eddy diffusivity of temperature is equal to that of salt, which implicitly assumes that seawater has a stable stratification [8]. Partly because of its relatively simple algebraic expression, Nikishov's spectrum has been widely used in theoretical calculations [9–12]. Indeed, the eddy diffusivity of temperature and salinity are different from each other in most underwater regions [7,13], and the spatial power spectrum of turbulent fluctuations of the seawater refraction index has been given by Elamassie that includes an eddy diffusivity ratio [7]. However, Elamassie's theory of oceanic spectrum only worked for infinity outer scale and did not include the effects of outer scale oceanic turbulence. Recently, a spatial power spectrum of unstable stratification oceanic turbulence has been proposed as an explicit function of the outer scale factor [14]. By considering the effect of the outer scale turbulence, this spectrum agrees well with the experimental data in all wavenumber regions.

On the other hand, motivated by the fact that OAM states of vortex beams are discrete, integer-valued and construct a theoretical infinite-dimensional Hilbert space [15], the entanglement of OAM has been demonstrated to carry more information in optical communication [16,17]. It is possible to obtain entangled OAM states via spontaneous parametric down-conversion [18] and transport through turbulence [19,20]. OAM entanglement not only presents an approach to enhance information capacity [21] but also promises

strong robustness against decoherence effects [22] and higher security [23]. However, the transmission of OAM entanglement states in free space is challenging [20]. The entanglement of OAM would be destroyed by beam wandering, wavefront degradation and scintillation induced by turbulence [24]. There are many efforts toward OAM entanglement propagation through turbulence. By introducing the phase correlation length of Laguerre–Gaussian (LG) modes, the decay of OAM entanglement states upon propagation through atmospheric turbulence has been discussed [25]. It turns out that the entanglement of photonic OAM shows a universal exponential decay in weak turbulence. Moreover, the effects of non-Kolmogorov atmospheric turbulence on bi-photon entangled OAM states have been discussed by means of LG modes [26]. In the above studies, LG beams possessing a well-defined OAM serve as a common option for the light source. In fact, Airy beams have non-diffraction [27], autofocusing [4,28] and self-healing [29,30] properties, providing considerable potential as a bi-photon entangled UOC link. The propagation dynamic of Airy beams has been proven in simulations to mitigate the OAM degradation and reduce the crosstalk induced by turbulence [31,32]. Recently, the spatially entangled Airy bi-photon has been generated experimentally and propagated in a vacuum [33]. To apply the entangled Airy source in the UOC link, the investigation of entangled Airy beams in oceanic turbulence is imminent.

In this paper, we demonstrate the propagation of the OAM of bi-photon entangled Airy beams through unstable oceanic turbulence. The semi-classical method is extended into a bi-photon case, and the relative detection probability of bi-photon entangled Airy beams is developed. Based on the general integrals, the analytical expression of the spatial coherence radius of a spherical wave propagating in unstably stratified oceanic turbulence is derived. Analyzing the results of numerical simulations, we compare the bi-photon entangled system and non-entangled ones and study how OAM modes of the bi-photon entangled Airy beams are affected by specific parameters of beam and turbulence. Through analytical simulations under various parameter settings, entangled Airy beams show stronger robustness to oceanic turbulence than single ones.

2. Methods

The sketch of a bi-photon entangled UOC link is illustrated in Figure 1. For non-trivial subspace ($m_0 \neq 0$), where m_0 is a general symbol for the OAM number, we assume that the initial state of the bi-photon Airy beams is an entangled Bell-like state [19,34]:

$$|\Psi\rangle = \mu|m_1, m_2\rangle + \nu| - m_1, -m_2\rangle, \tag{1}$$

where $m_1 = m_0$, $m_2 = -m_1$ for the conversation of momentum, $|m_i\rangle$ represents a single photon OAM eigenmode of an Airy mode, m_i is the OAM quantum number corresponding to the OAM $m_i\hbar$, the subscript $i(i = 1, 2)$ is used to label two different channels of the two photons and μ and ν denote probability amplitudes that are subject to $|\mu|^2 + |\nu|^2 = 1$. As the constituent photons launched with equal probability ($\mu = \nu$), the maximal entanglement occurs for the initial bi-photon.
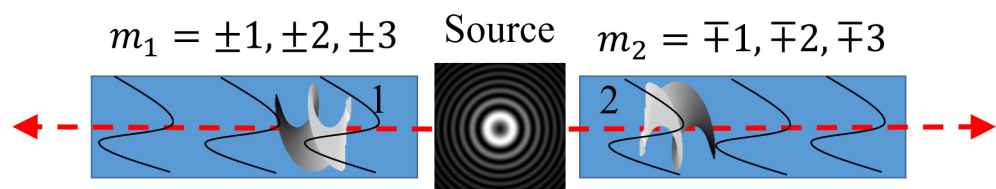

Figure 1. Sketch of a thought experiment involving bi-photon propagation through independent turbulence paths 1 and 2.

Using cylindrical representation and inserting the completeness relation $\int |\vec{r}_i\rangle \langle \vec{r}_i| \mathrm{d}\vec{r}_i = I$, one can obtain the probability of the joint OAM measurement at propagation distance z as [35]

$$
\begin{aligned}
p(m_1 m_2|\Psi) &= \langle m_1 m_2|\Psi\rangle\langle\Psi|m_1 m_2\rangle \\
&= \int\int \langle m_1 m_2|\vec{r}_1 \vec{r}_2\rangle\langle\vec{r}_1 \vec{r}_2|\Psi\rangle \mathrm{d}\vec{r}_1 \mathrm{d}\vec{r}_2 \int\int \langle\Psi|\vec{r}_1' \vec{r}_2'\rangle\langle\vec{r}_1' \vec{r}_2'|m_1 m_2\rangle \mathrm{d}\vec{r}_1' \mathrm{d}\vec{r}_2'
\end{aligned}
\tag{2}
$$

with $\vec{r}_i = (r_i, \varphi_i, z)$, $r_i = |\mathbf{r}_i|$ is the radial distance from the axis and $\mathbf{r}_i = (x_i, y_i)$ is the two-dimensional vector. The joint OAM detection probability is then given by the ensemble average [36] of Equation (2) as

$$
p_{m_1 m_2}(z) = \int \cdots \int r_1 r_2 \mathrm{d}r_1 \mathrm{d}r_2 \mathrm{d}\varphi_1 \mathrm{d}\varphi_1' \mathrm{d}\varphi_2 \mathrm{d}\varphi_2' C_\Psi \prod_{i=1}^{2} \frac{\exp[-\mathrm{i}m_i(\varphi_i - \varphi_i')]}{2\pi}
\tag{3}
$$

where $C_\Psi = \langle\Psi(r_1, r_2, \varphi_1, \varphi_2, z)\Psi^*(r_1, r_2, \varphi_1', \varphi_2', z)\rangle$ is defined as the rotational field correlation of the bi-photon. For convenience, we set $\Delta\varphi_i = \varphi_i - \varphi_i'$ and $\bar{\varphi}_i = (\varphi_i + \varphi_i')/2$ to rewrite Equation (3) as

$$
p_{m_1 m_2}(z) = \int \cdots \int \left(\prod_i r_i \mathrm{d}r_i \Delta\varphi_i \mathrm{d}\bar{\varphi}_i \right) C_\Psi(r_1, r_2, \Delta\varphi_1, \Delta\varphi_2, \bar{\varphi}_1, \bar{\varphi}_2, z) \frac{\exp(-\mathrm{i}\sum_i m_i \Delta\varphi_i)}{4\pi^2}.
\tag{4}
$$

Generalizing the semi-classical approach [36] to bi-photon entangled case, the bi-photon entangled Airy beams $\Psi(r_1, r_2, \varphi_1, \varphi_2, z)$ is given by

$$
\begin{aligned}
\Psi(r_1, r_2, \varphi_1, \varphi_2, z) &= R^{|m_1|}(r_1, z) R^{|m_2|}(r_2, z) \frac{\exp[\mathrm{i}\phi(r_1, r_2, \varphi_1, \varphi_2, z)]}{2\pi} \\
&\times \{\mu\exp[\mathrm{i}m_1(\varphi_1 - \varphi_2)] + \nu\exp[\mathrm{i}m_2(\varphi_1 - \varphi_2)]\},
\end{aligned}
\tag{5}
$$

where $\phi(r_1, r_2, \varphi_1, \varphi_2, z)$ is the phase perturbation induced by turbulence, which gives rise to the crosstalk of OAM, and $R^{|m_i|}(r_i, z)$ is the radial component of Airy beam. Substituting Equation (5) into Equation (4), the final expression of the joint detection probability is derived as

$$
\begin{aligned}
p_{m_1 m_2}(z) &= \int_0^\infty \int_0^\infty \left| R^{|m_1|}(r_1, z) R^{|m_2|}(r_2, z) \right|^2 \\
&\times \left[|\mu|^2 \Theta(r_1, r_2, m_1^-, m_2^+, z) + |\nu|^2 \Theta(r_1, r_2, m_1^+, m_2^-, z) \right] r_1 r_2 \mathrm{d}r_1 \mathrm{d}r_2,
\end{aligned}
\tag{6}
$$

where $m_i^- = m_i - m_0$, $m_i^+ = m_i + m_0$, and $\Theta(x)$ represents the circular harmonic transformation of the rotational coherence function [36].

Given to Markov approximation, we consider the turbulent channels 1 and 2 are independent [25]. The relative version of the detection probability is calculated to study the influence of oceanic turbulence on the entangled bi-photon due to the existence of the launching probability at the source plane. By partially tracing the joint detection probability $p_{m_1 m_2}(z)$, and considering the probability of launching $|m_1\rangle$, the relative detection probability $p_{rm_1}(z)$ of the signal photon reads

$$
p_{rm_1}(z) = \frac{\sum_{m_2} p_{m_1 m_2}(z)}{|\mu|^2} = p_1(m_1^-, z) + \frac{|\nu|^2}{|\mu|^2} p_1(m_1^+, z),
\tag{7}
$$

where $p_i(m_i, z)$ is the detection probability of measuring the OAM of a single-photon Airy beam for a receiver with the aperture diameter D

$$
p_i(m_i, z) = \int_0^{D/2} \left| R^{|m_i|}(r_i, z) \right|^2 r_i \Theta(r_i, m_i, z) \mathrm{d}r_i,
\tag{8}
$$

for non-normalized wavefunctions, the normalization of Equation (8) must be performed via $p_i(m_i, z)/\sum_{m_i} p_i(m_i, z)$. Without a loss in generality, we shall denote that the relative

detection probability for faithful propagation is $p_{rm_1}(z)$ (i.e., $m_1 = m_0$) and the crosstalk probability that detects OAM modes $m_i = \pm m_0 + \Delta m_i$ is $p_{\Delta m_i}(z)$. Moreover, Equation (8) is given under Rytov approximation [5], where the effects of the oceanic turbulence on the OAM beam are simplified as only phase disturbance. Thus the application of our model is theoretically limited to the weak fluctuation region. When launching photon i with probability 1 ($\mu = 1$), the second term in Equation (7) is 0. In this case, Equation (7) is equivalent to Equation (8).

Comparing the relative detection probability of a single photon in Equation (8), an extra item $|\nu|^2 p_1(m_1^+, z)/|\mu|^2$ comes out in Equation (7) describing the relative detection probability of a bi-photon. Take OAM state $|m_1\rangle$ as an example, $p_{rm_1}(z) \geq p_1(m_1, z)$ due to the detection probability always being a non-negative real number. Physically, the quantity $|\nu|^2 p_1(m_1^+, z)/|\mu|^2$ represents the transition of an OAM state $|m_2\rangle$ caused by oceanic turbulence, which results in the elevation of the relative probability $p_{rm_1}(z)$.

For an aperture-truncated Airy beam, $R^{|m_i|}(r_i, z)$ is given by [28]

$$R^{|m_i|}(r_i, z) = -\sqrt{2\pi}\frac{ik}{z}\omega_0(r_0 - \omega_0 a^2)\exp\left(ik\frac{r_i^2}{2z} + \frac{a^3}{3}\right)J_{m_i}\left(\frac{kr_i r_0}{z}\right), \tag{9}$$

where k is the wave number and is related to the wavelength λ in general by $k = 2\pi/\lambda$, r_0 and a are the radius of the main ring and the exponential truncation parameter, respectively, ω_0 is the arbitrary transverse scale [37] and $J_n(x)$ is the first-kind Bessel function of the nth order.

To further understand the effects of the significant parameters of Airy modes on the beam structure, the transverse intensity distributions of Airy beams in a vacuum for different ω_0, r_0 and a at the source plane ($z = 0$) are plotted in Figure 2. The simulation is conducted by the software of Mathematica 13.0. It is clear to see that the beam size of the Airy beam increases with the increasing ω_0, and the dark spot at the center spreads with the increment of r_0 simultaneously (Figure 2b,c). Moreover, as $a > 1$, the intensity distribution of the Airy beam evolves into a Gaussian distribution [38], as shown in Figure 2d.
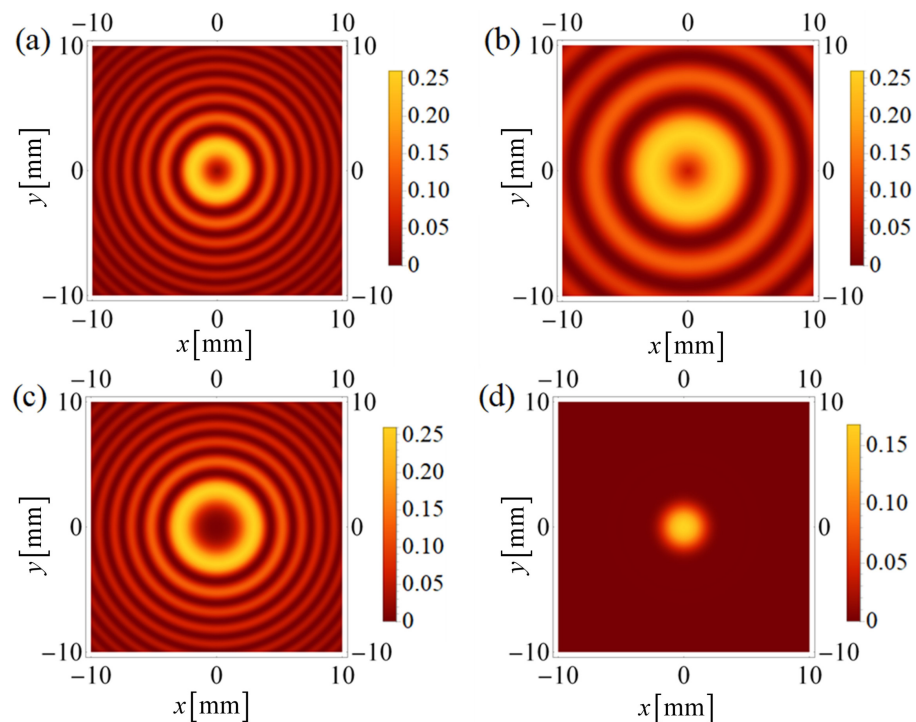

Figure 2. Intensity distribution for Airy beams in a vacuum of different beam parameters. Compared with (**a**) $\omega_0 = 1$ mm, $r_0 = 1$ mm, $a = 0.05$, the different parameters in (**b**–**d**) are: (**b**) $\omega_0 = 2$ mm, (**c**) $r_0 = 2$ mm and (**d**) $a = 1.1$.

We now proceed to discuss how oceanic turbulence influences the OAM of bi-photon entangled Airy beams. Based on the quadratic approximation of the wave structure function [5], the circular harmonic transformation of the rotational coherence function $\Theta(x)$ becomes

$$\Theta(r_i, m_i, z) = \frac{1}{2\pi} \int_0^{2\pi} \exp\left[-\frac{2r_i^2 - 2r_i^2\cos(\Delta\varphi_i)}{\rho_{oc}^2} - im_i\Delta\varphi_i\right] d\Delta\varphi_i, \tag{10}$$

where $\Delta\varphi_i = \varphi_i - \varphi_i'$, and ρ_{oc} is the spatial coherence radius of a spherical wave propagating in the oceanic turbulence calculated as [3]

$$\rho_{oc}^{-2} = \frac{1}{3}\pi^2 k^2 z \int_0^\infty \kappa^3 \Phi_n(\kappa) d\kappa. \tag{11}$$

$\Phi_n(\kappa)$ in Equation (11), a theoretical description of the statistical characteristics of a wave propagating through optical turbulence, denotes the power spectrum of refractive fluctuations [5,8] and is related to the magnitude of the wave number vector κ. In a the real ocean circumstance, the eddy diffusivity ratio of temperature to salt is not equal to unity. When unstable stratification exists, and outer scale effects cannot be ignored in oceanic turbulence, the spectrum is given by [14]

$$\Phi_n(\kappa) = \frac{\epsilon^{-1/3}\beta\chi_T A^2[1 + C_1(\kappa\eta)^{2/3}]}{4\pi(\kappa^2 + \kappa_0^2)^{11/6}}$$
$$\times \left\{\exp\left[-\frac{(\kappa\eta)^2}{R_T^2}\right] + \frac{1}{\omega^2\theta}\left[-\frac{(\kappa\eta)^2}{R_S^2}\right] - \frac{1+\theta}{\omega\theta}\left[-\frac{(\kappa\eta)^2}{R_{TS}^2}\right]\right\}, \tag{12a}$$

$$R_j = \sqrt{3}Q^{-3/2}\left(W_j - \frac{1}{3} + \frac{1}{9W_j}\right)^{3/2}, \tag{12b}$$

$$W_j = \left\{\left[\frac{Pr_j^2}{(6\beta Q^{-2})^2} - \frac{Pr_j}{81\beta Q^{-2}}\right]^{1/2} - \left(\frac{1}{27} - \frac{Pr_j}{6\beta Q^{-2}}\right)\right\}^{1/3}, \tag{12c}$$

where $j = T, S, TS$ refers to temperature fluctuations, salinity fluctuations and coupling fluctuations, R_j and W_j are dimensionless constants that vary with different "j", $\kappa_0 = 1/L_0$ is the spatial cutoff frequency, L_0 and η are the outer- and inner-scale of turbulence, respectively, ϵ is the rate of dissipation of kinetic energy per unit mass of fluid, β is the Obukhov–Corrsin constant, χ_T represents the dissipation rate of mean-squared temperature, $A = 2.6 \times 10^{-4}$ L/deg, $Q = 2.5$ is a non-dimensional constant, Pr_j is the Prandal number with $Pr_{TS} = 2Pr_T Pr_S/(Pr_T + Pr_S)$, $C_1 = 2.35$ is a free parameter, ω defines the ratio of temperature and salinity contributions to the refractive index spectrum that varies from -5 to 0 and $\theta = K_T/K_S$ is the eddy diffusivity ratio where K_T and K_T denote the eddy thermal diffusivity and the diffusion of salinity, respectively. According to Ref. [7], we have the relationship of ω and θ in the unstable stratification as

$$\theta = \frac{|\omega|}{R_F} \approx \begin{cases} \left(1 - \sqrt{(|\omega|-1)/|\omega|}\right)^{-1} & |\omega| \geq 1 \\ 1.85|\omega| - 0.85 & 0.5 \leq |\omega| \leq 1' \\ 0.15|\omega| & |\omega| \leq 0.5 \end{cases} \tag{13}$$

with R_F is the eddy flux ratio.

For a spherical wave propagating through unstably stratified oceanic turbulence, the spatial coherence radius is obtained by substituting the modified spectrum $\Phi_n(\kappa)$ into Equation (11) as

$$
\rho_{\text{oc}}^{-2} = \frac{1}{3}\pi^2 k^2 z \epsilon^{-1/3} \chi_T \beta A^2 \int_0^\infty \kappa^3 \frac{1 + C_1(\kappa\eta)^{2/3}}{4\pi(\kappa^2 + \kappa_0^2)^{11/6}}
$$
$$
\times \left\{ \exp\left[-\frac{(\kappa\eta)^2}{R_T^2}\right] + \frac{1}{\omega^2\theta}\left[-\frac{(\kappa\eta)^2}{R_S^2}\right] - \frac{1+\theta}{\omega\theta}\left[-\frac{(\kappa\eta)^2}{R_{TS}^2}\right] \right\} \mathrm{d}\kappa, \tag{14}
$$

based on the following two integral expressions

$$
\int_0^\infty \frac{\kappa^3}{(\kappa^2 + \kappa_0^2)^{11/6}} \exp\left[-\frac{(\kappa\eta)^2}{R_j^2}\right] \mathrm{d}\kappa
$$
$$
= \frac{\exp\left(\frac{\eta^2\kappa_0^2}{R_j^2}\right)\left(5 + 6\frac{\eta^2\kappa_0^2}{R_j^2}\right)\Gamma\left(\frac{1}{6}, \frac{\eta^2\kappa_0^2}{R_j^2}\right) - 6\left(\frac{\eta^2\kappa_0^2}{R_j^2}\right)^{1/6}}{10\left(\frac{\eta^2}{R_j^2}\right)^{1/6}}, \tag{15a}
$$

$$
\int_0^\infty \frac{\kappa^{11/3}}{(\kappa^2 + \kappa_0^2)^{11/6}} \exp\left[-\frac{(\kappa\eta)^2}{R_j^2}\right] \mathrm{d}\kappa
$$
$$
= \frac{\sqrt{\pi}\kappa_0}{2}\left[\frac{{}_1\mathrm{F}_1\left(\frac{11}{6}; \frac{1}{2}; \frac{\eta^2\kappa_0^2}{R_j^2}\right)}{\sqrt{\frac{\eta^2\kappa_0^2}{R_j^2}}} - 2\frac{\Gamma\left(\frac{7}{3}\right){}_1\mathrm{F}_1\left(\frac{7}{3}; \frac{3}{2}; \frac{\eta^2\kappa_0^2}{R_j^2}\right)}{\Gamma\left(\frac{11}{6}\right)} \right], \tag{15b}
$$

where ${}_1\mathrm{F}_1(\alpha; \gamma; \tau)$ is the confluent hypergeometric function, the final expression of the spatial coherence radius of a spherical wave propagating in unstably stratified oceanic turbulence is derived as

$$
\rho_{\text{oc}} = \left\{ 0.262\beta A^2 k^2 z \epsilon^{-1/3} \frac{\chi_T}{\omega^2\theta}\left[\omega^2\theta\Lambda_T + \Lambda_S - \omega(1+\theta)\Lambda_{TS}\right] \right\}^{-\frac{1}{2}}, \tag{16}
$$

with

$$
\Lambda_j = \frac{\kappa_0^{1/3} e^{\vartheta_j}\left(5 + 6\vartheta_j\right)}{10\vartheta_j^{1/6}}\Gamma\left(\frac{1}{6}, \vartheta_j\right) - \frac{3}{5}\kappa_0^{1/3}
$$
$$
+ \frac{C_1\sqrt{\pi}}{2}\eta^{2/3}\kappa_0\left[\frac{{}_1\mathrm{F}_1\left(\frac{11}{6}; \frac{1}{2}; \vartheta_j\right)}{\sqrt{\vartheta_j}} - 2\frac{\Gamma\left(\frac{7}{3}\right)}{\Gamma\left(\frac{11}{6}\right)}{}_1\mathrm{F}_1\left(\frac{7}{3}; \frac{3}{2}; \vartheta_j\right) \right], \tag{17}
$$

where $\vartheta_j = \left[\eta/(L_0 R_j)\right]^2$ is a turbulence factor determined by the inner- and outer scale of oceanic turbulence. From Equation (16), the effects of oceanic turbulence on the spherical wave can be regarded as the co-effects of temperature fluctuations, salinity fluctuations and coupling fluctuations.

3. Numerical Results and Discussion

In this section, the impacts of beam parameters and turbulence factors on the propagation of bi-photon entangled Airy beams in oceanic turbulence are numerically simulated. Unless otherwise specified, the basic parameters are given in Table 1.

Table 1. Parameter values used in the simulations.

Parameters	Value
OAM number m_0	1
Wavelength λ	417 nm
Exponential truncation parameter a	0.05
Arbitrary transverse scale ω_0	1 mm
Radius of the main ring r_0	1 mm
Aperture diameter D	0.06 m
Inner scale η	1 mm
Outer scale L_0	10 m
Obukhov-Corrsin constant β	0.72
Dissipation rate of kinetic energy per unit mass of fluid ϵ	1.7×10^{-5} m^2/s^3
Dissipation rate of mean-squared temperature χ_T	1.2×10^{-8} K^2/s
Ratio of temperature and salinity contributions ϖ	-2
Prandal number Pr_s	700
Prandal number Pr_T	7

Figure 3a shows a plot of the relative detection probability and crosstalk probability as a function of the initial probability amplitude μ at a fixed propagation distance. The plot detail of Figure 3a is presented in Appendix A. By taking different values of μ in Equation (7), Figure 3a demonstrates the relationship between OAM entanglement and OAM probability. The maximum value of the relative detection probability and the minimum value of the crosstalk probability of the signal photon are both located at $\mu = 1/\sqrt{2}$, which correspond to the maximal entanglement. With the increment of entanglement, the noise induced by turbulence in the UOC system is suppressed, and the signal becomes more distinguishable for receivers [26]. To evaluate the impacts of bi-photon entanglement on the OAM propagation in unstable oceanic turbulence, $(p_{rm_1} - p_{m_0})/p_{m_0}$ is calculated to quantify the improvement of the bi-photon entanglement in comparison with a single photon under the same UOC link, where p_{m_0} denotes the single photon detection probability in Equation (8). In what follows, we discuss the maximally entangled case of p_{rm_1}, which is calculated according to Equation (7). As shown in Figure 3b, the smaller the OAM quantum number m_0 is, the more pronounced the performance of the UOC link based on bi-photon entanglement improves. The maximal improvement reaches 62%, especially in the case $m_0 = 1$. However, this improvement decreases with the increment of the initial OAM quantum number, and Figure 3b shows only a 17% improvement in the relative detection probability of the UOC link when $m_0 = 5$. It reveals that bi-photon entangled Airy beams with smaller m_0 are more robust to oceanic turbulence. Concurrently, the generation of vortex beams with a small m_0 is easier than that with a large m_0 in practical applications [39]. Therefore, the entangled Airy bi-photon with a small OAM number is the preferable light source in a practical UOC link.

For OAM-based systems, information is encoded in the entire Hilbert space, where the turbulence effects, such as the fluctuations of the refractive index of the water flow [40], would cause the quantum state of photons to be partially transferred into other orthogonal complements, resulting in the mode scattering of OAM, or generally, the crosstalk, which is a disadvantage compared to polarization-based systems. The relative detection probability of a single photon and bi-photon entangled Airy beams are plotted in Figure 4, where we give no consideration to the trivial case $m_0 = 0$ according to Equation (1). For short-distance communication, as shown in Figure 4a,c, the signal still remains distinguishable for the crosstalk only existing on the immediately adjacent channels. As the propagation distance increases, for example, $z = 50$ m (as shown in Figure 4b,d), the crosstalk is conspicuous in all the observed channels. For large values of transmitted $|m_1\rangle$, oceanic turbulence makes the OAM state of the beam more prone to spread and the channel more vulnerable. Figure 4b,d shows that the OAM distribution of bi-photon entanglement for low-order OAM states is effectively enhanced in comparison with that of a single photon, while the phenomenon

gradually disappears as the OAM number increases. With the increase in the initial m_0, the gap between m_1 and m_2 in Hilbert space becomes larger. Thus the mutual transfer is much harder than that for a smaller m_0. For example, $m_0 = \pm 10$, the probability of $|m_2\rangle$ transferred to $|m_1\rangle$ will probably be negligible, while the transition probability is an essential component of the $p_{rm_1}(z)$ in the case $m_0 = \pm 1$. This result also explains why the improvement in entanglement on the relative detection probability decreases with increases in OAM carried by an Airy beam in Figure 3b.
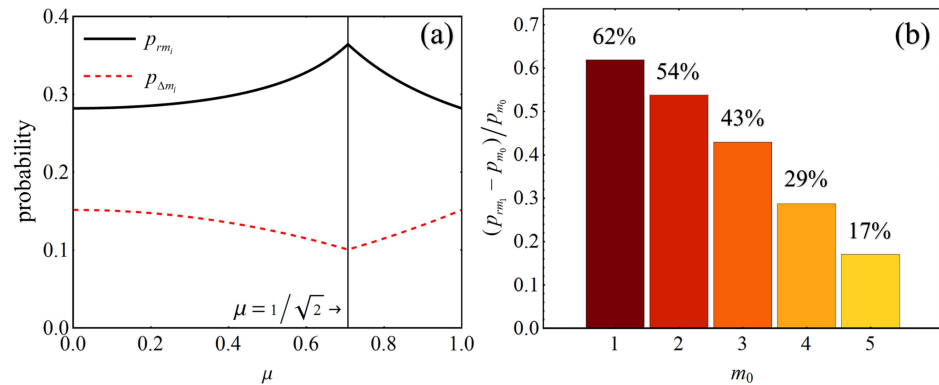

Figure 3. (**a**) Relative detection probability and crosstalk probability of the signal photon versus initial probability amplitude μ ($z = 50$ m, $\Delta m_i = 1$); (**b**) $(p_{rm_1} - p_{m_0})/p_{m_0}$ versus OAM quantum numbers m_0 ($z = 100$ m).
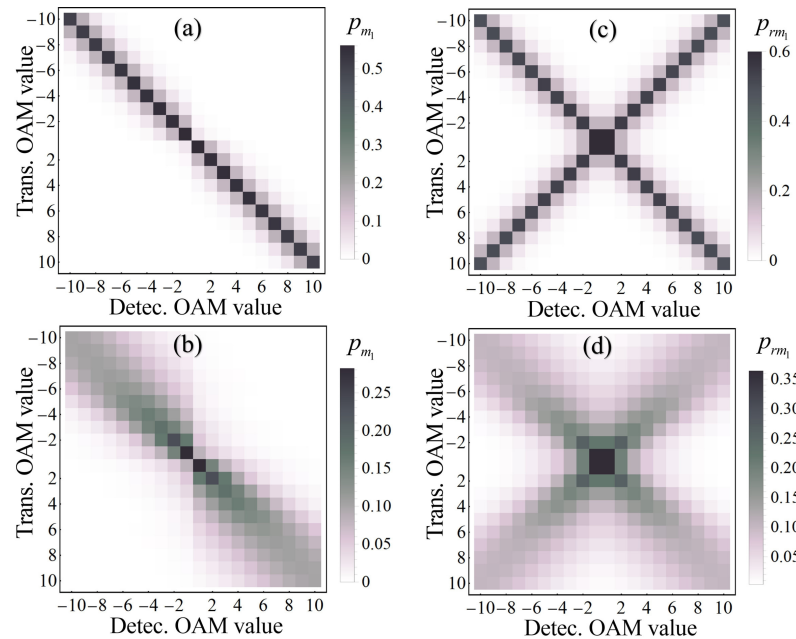

Figure 4. Relative detection probability under oceanic turbulence of the single photon (**a**,**b**) and bi-photon entangled Airy beams (**c**,**d**) (for OAM, $|m_1\rangle$ detections are plotted as the leading diagonal elements, while $|m_2\rangle$ detections as the minor diagonal elements). With a propagation distance from $z = 10$ m (**a**,**c**), increasing to $z = 50$ m (**b**,**d**).

In a practical UOC system, parameter selection of the light source attracts extensive interest. Figure 5a shows the evolution of the relative detection probability p_{rm_1} as the propagation distance increases for different wavelengths λ. Here, the values of λ are selected from 417, 477 and 532 nm due to their small absorption loss under the sea. It can be seen from Figure 5a that p_{rm_1} increases with λ slightly. Airy beams with a shorter wavelength have a larger wave number that is more susceptible to turbulent fluctuations [41]. Moreover, we note that at propagation distance $z = 100$ m, the relative detection probabilities p_{rm_1} of

different λ are approximately the same, which means that the communication wavelength could be equally optional at this distance. To investigate the effect of the main ring radius r_0 on the OAM of bi-photon entangled Airy beams, we plot Figure 5b. As r_0 increases from 1 to 5 mm, the detection probability p_{rm_1} rockets. The main ring radius r_0 determines the energy characteristics of Airy beams larger than r_0 corresponding to larger maximal intensity [42], thus elevating the detection probability. As we further increase r_0 to 25 mm, the probability p_{rm_1} becomes saturated. It indicates that the main ring radius of bi-photon entangled Airy beams and the design of the UOC system should be appropriately matched. While a larger main ring radius does not contribute to the increment of the detection probability, fewer fluctuations of detection probability are observed for a larger r_0 in $z < 100$ m. This effect is caused by the dispersion degree of the Airy beam being smaller so that the detection over different distances is more stable [43].
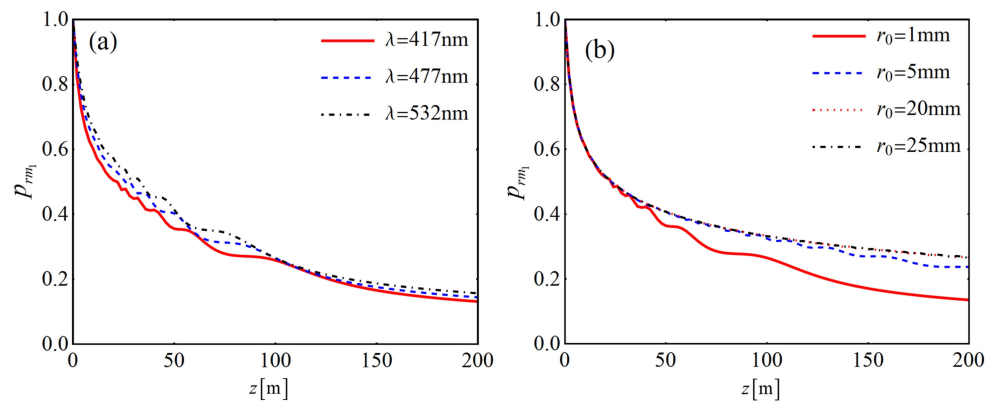

Figure 5. Relative detection probability of signal photon versus propagation distance for different (**a**) wavelengths λ and (**b**) main ring radius r_0.

The basic conditions of oceanic turbulence are essential for the design of an UOC system. Figure 6 illustrates the effect of the ratio of temperature and salinity contributions to the refractive index ϖ on the relative detection probability p_{rm_1}. Different from atmospheric turbulence, both temperature and salinity fluctuations are important factors in determining OAM transmission in oceanic turbulence. As ϖ varies from 0 to -5, the oceanic turbulence turns from salinity-induced dominated into temperature-induced dominated [9]. For the same distance, p_{rm_1} increases as ϖ approaches -5 and gains its maximum value at $\varpi = -5$. Physically it reveals that the OAM of bi-photon entangled Airy beams will experience fewer adverse effects of turbulence in temperature-induced dominated oceanic turbulence than salinity-induced dominated oceanic turbulence.
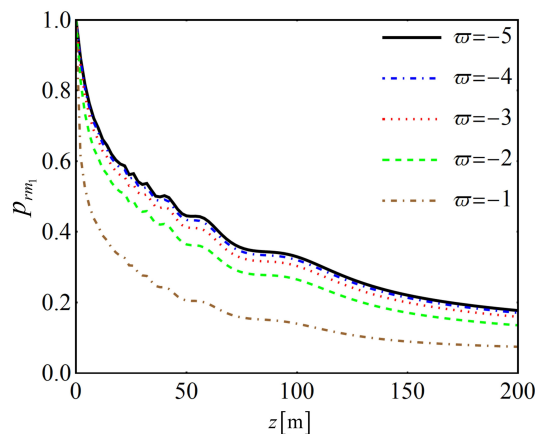

Figure 6. Relative detection probability of signal photon versus propagation distance for different ratios of temperature and salinity contributions to the refractive index ϖ.

Except for the ratio φ, oceanic turbulence is also affected by turbulence factors, including L_0, η, χ_T and ϵ, whose influences on the entangled Airy beams are illustrated in Figure 7. Since our employed oceanic spectrum taking outer scale of turbulence L_0 into consideration agrees well with the experimental data in all wavenumber regions, we investigate the impacts of L_0 and η on the OAM propagation. The outer- and the inner-scales define the scale sizes of turbulence eddies in the inertial range. The effective turbulence eddies in the inertial range would decrease with the increment of η. Thus the beam scattering is reduced [12], corresponding to our result in Figure 7a, where p_{rm_1} increases when η increases. By comparing η and L_0, we note that L_0 has less influence on OAM detection. Then, we demonstrate the relative detection probability against different dissipation rates of mean-squared temperature χ_T and different dissipation rates of turbulent kinetic energy per unit mass of fluid in Figure 7b. The probability decreases with increasing χ_T and decreasing ϵ. It generally illustrates that a larger χ_T and a smaller ϵ correspond to stronger oceanic turbulence and, thus, a smaller detection probability [14].

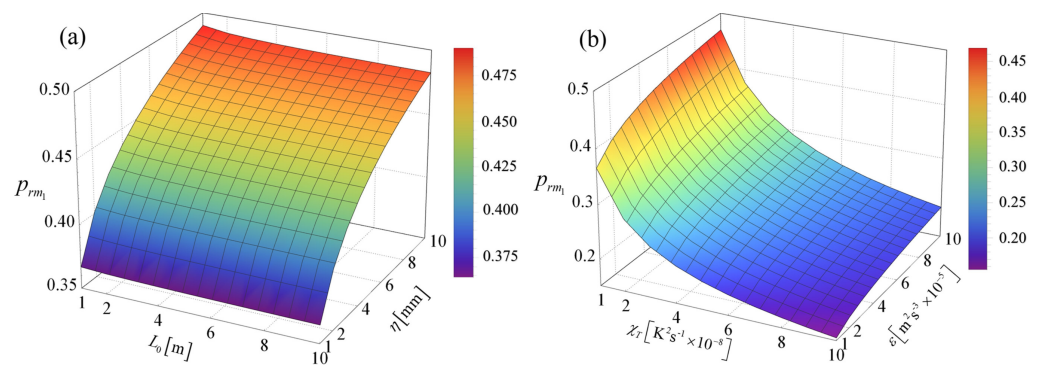**Figure 7.** Relative detection probability of signal photon under (**a**) different outer scale turbulences L_0 and inner-scale turbulences η; (**b**) different dissipation rates of mean-squared temperature χ_T and different dissipation rates of kinetic energy per unit mass of fluid ϵ ($z = 50$ m).

4. Conclusions

In this paper, we have proposed a theoretical model describing the OAM of bi-photon entangled Airy beams propagating through unstable stratifications of oceanic turbulence. We extend the theory of quantifying single photon OAM communication to obtain the relative detection probability in a bi-photon entangled case and express the bi-photon detection probability as two parts of a single photon detection probability. The analytical expression of the spatial coherence radius of a spherical wave in an unstably stratified oceanic turbulence is derived. Our results demonstrate that bi-photon entangled Airy beams obtain larger relative detection probability than non-entangled ones and are the largest for the maximally entangled case, which is caused by the modal transfer of the bi-photon. The order of Airy beams plays a key role in the detection. For low-order bi-photon entangled Airy beams, OAM entanglement effectively suppresses the crosstalk and improves the relative detection probability. The lowest-order modes of OAM carried by the bi-photon entangled Airy beams exhibit stronger resistance against oceanic turbulence. Consequently, up to a 62% improvement is achieved over a distance of 100 m compared to the same measurement for the single photon system. To detect more initial OAM modes at receivers, bi-photon entangled Airy beams with a larger wavelength λ and main ring radius r_0 are preferable. Moreover, a larger main ring radius r_0 is also found to help reduce the fluctuations in the relative detection probability in oceanic turbulence. The discussions with respect to oceanic turbulence reveal that bi-photon entangled Airy beams in the turbulence of temperature-dominated fluctuations are less affected. The performance of a UOC system is related to oceanic turbulence with a larger inner-scale η, larger dissipation rate of turbulent kinetic energy per unit mass of fluid ϵ and a smaller rate of the dissipation

of mean-squared temperature χ_T. These findings may be useful in a UOC link based on the OAM of bi-photon entangled Airy beams.

In this work, we study the probability distribution of the entangled Airy beams in weak-strength turbulence. One of our future works will be to disclose how entangled Airy beams evolve in all strength regions of turbulence. The recent report that states that the auto-focus of Airy beam is reported to help reduce OAM crosstalk [31] will motivate the direction of our future work to investigate the interaction effects between auto-focus and entanglement.

Author Contributions: Conceptualization, D.Y., Y.Z. and Z.H.; methodology, D.Y. and Y.Z.; software, D.Y., Z.Y. and W.W.; validation, D.Y., Z.H. and Y.Z.; formal analysis, D.Y. and Y.Z.; investigation, D.Y.; resources, D.Y.; data curation, D.Y. and Z.Y.; writing—original draft preparation, D.Y.; writing—review and editing, D.Y., Z.H. and Y.Z.; visualization, D.Y., Z.Y. and W.W.; supervision, Z.H. and Y.Z.; project administration, Y.Z. All authors have read and agreed to the published version of the manuscript.

Institutional Review Board Statement: Not applicable.

Informed Consent Statement: Not applicable.

Data Availability Statement: Not applicable.

Conflicts of Interest: The authors declare no conflict of interest.
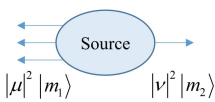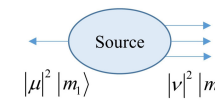
Appendix A. Plot Detail of Figure 3a

Case	$1/\sqrt{2} \leq \mu \leq 1$	$0 \leq \mu \leq 1/\sqrt{2}$
Sketch	Source $\lvert\mu\rvert^2 \lvert m_1\rangle$ $\lvert\nu\rvert^2 \lvert m_2\rangle$	Source $\lvert\mu\rvert^2 \lvert m_1\rangle$ $\lvert\nu\rvert^2 \lvert m_2\rangle$
Signal OAM mode	$\lvert m_1\rangle$	$\lvert m_2\rangle$
Relative signal probability	$p_{rm_1}(z) = \dfrac{\sum\limits_{m_2} p_{m_1 m_2}(z)}{\lvert\mu\rvert^2}$	$p_{rm_2}(z) = \dfrac{\sum\limits_{m_1} p_{m_1 m_2}(z)}{\lvert\nu\rvert^2}$
Crosstalk probability	$p_{\Delta m_1}(z) = \sum\limits_{m_2} p_{m_1 m_2}(z)$	$p_{\Delta m_2}(z) = \sum\limits_{m_1} p_{m_1 m_2}(z)$

Figure A1. Plot detail of Figure 3a.

References

1. Baghdady, J.; Miller, K.; Morgan, K.; Byrd, M.; Osler, S.; Ragusa, R.; Li, W.; Cochenour, B.M.; Johnson, E.G. Multi-gigabit/s underwater optical communication link using orbital angular momentum multiplexing. *Opt. Express* **2016**, *24*, 9794–9805. [CrossRef] [PubMed]
2. Chen, Y.; Shen, W.G.; Li, Z.M.; Hu, C.Q.; Quan, Y.; Jiao, Z.; Gao, J.; Cao, M.M.; Sun, K.; Jin, X.M. Underwater transmission of high-dimensional twisted photons over 55 meters. *PhotoniX* **2020**, *1*, 1–11. [CrossRef]
3. Zhan, H.; Wang, L.; Wang, W.; Zhao, S. Experimental analysis of adaptive optics correction methods on the beam carrying orbital angular momentum mode through oceanic turbulence. *Optik* **2021**, *240*, 166990. [CrossRef]
4. Wang, J.; Wang, X.; Peng, Q.; Zhao, S. Propagation characteristics of autofocusing Airy beam with power exponential phase vortex in weak anisotropic oceanic turbulence. *J. Mod. Opt.* **2021**, *68*, 1–7. [CrossRef]
5. Andrews, L.C.; Phillips, R.L. *Laser Beam Propagation Through Random Media*; SPIE Digital Library: Bellingham, WA, USA, 2005.
6. Yao, J.; Zhang, Y.; Wang, R.; Wang, Y.; Wang, X. Practical approximation of the oceanic refractive index spectrum. *Opt. Express* **2017**, *25*, 23283–23292. [CrossRef] [PubMed]

7. Elamassie, M.; Uysal, M.; Baykal, Y.; Abdallah, M.; Qaraqe, K. Effect of eddy diffusivity ratio on underwater optical scintillation index. *J. Opt. Soc. Am. A* **2017**, *34*, 1969–1973. [CrossRef]

8. Nikishov, V.; Nikishov, V. Spectrum of Turbulent Fluctuations of the Sea-Water Refraction Index. *Int. J. Fluid Mech. Res.* **2000**, *27*, 82–98. [CrossRef]

9. Lu, W.; Liu, L.; Sun, J. Influence of temperature and salinity fluctuations on propagation behaviour of partially coherent beams in oceanic turbulence. *J. Opt. A Pure Appl. Opt.* **2006**, *8*, 1052–1058. [CrossRef]

10. Lu, L.; Ji, X.; Baykal, Y. Wave structure function and spatial coherence radius of plane and spherical waves propagating through oceanic turbulence. *Opt. Express* **2014**, *22*, 27112–27122. [CrossRef]

11. Ata, Y.; Baykal, Y. Effect of anisotropy on bit error rate for an asymmetrical Gaussian beam in a turbulent ocean. *Appl. Opt.* **2018**, *57*, 2258–2262. [CrossRef]

12. Yu, L.; Zhang, Y. Analysis of modal crosstalk for communication in turbulent ocean using Lommel-Gaussian beam. *Opt. Express* **2017**, *25*, 22565–22574. [CrossRef] [PubMed]

13. Chapter 8 Waters of the World Ocean—ScienceDirect. *Elsevier Oceanogr. Ser.* **1975**, *11*, 305–334.

14. Li, Y.; Zhang, Y.; Zhu, Y. Oceanic spectrum of unstable stratification turbulence with outer scale and scintillation index of Gaussian-beam wave. *Opt. Express* **2019**, *27*, 7656–7672. [CrossRef]

15. Jabir, M.V.; Anwar, A.; Samanta, G.K. Controlling the biphoton orbital angular momentum eigenmodes using asymmetric pump vortex beam. *J. Opt.* **2018**, *21*, 1–4. [CrossRef]

16. Mair, A.; Vaziri, A.; Weihs, G.; Zeilinger, A. Entanglement of Orbital Angular Momentum States of Photons. *Nature* **2001**, *412*, 313–316. [CrossRef]

17. Mafu, M.; Dudley, A.; Goyal, S.; Giovannini, D.; Mclaren, M.; Padgett, M.; Konrad, T.; Petruccione, F.; Lütkenhaus, N.; Forbes, A. Higher-dimensional orbital-angular-momentum-based quantum key distribution with mutually unbiased bases. *Phys. Rev. A* **2013**, *88*, 032305. [CrossRef]

18. Walborn, S.; Oliveira, A.; Thebaldi, R.; Monken, C. Entanglement and conservation of orbital angular momentum in spontaneous parametric down-conversion. *Phys. Rev. A* **2005**, *69*, 023811. [CrossRef]

19. Hamadou Ibrahim, A.; Roux, F.; Mclaren, M.; Konrad, T.; Forbes, A. Orbital angular momentum entanglement in turbulence. *Phys. Rev. A* **2013**, *88*, 012312. [CrossRef]

20. Krenn, M.; Handsteiner, J.; Fink, M.; Fickler, R.; Zeilinger, A. Twisted photon entanglement through turbulent air across Vienna. *Proc. Natl. Acad. Sci. USA* **2015**, *112*, 14197–14201. [CrossRef]

21. Karpov, E.; Daems, D.; Cerf, N. Entanglement-enhanced classical capacity of quantum communication channels with memory in arbitrary dimensions. *Phys. Rev. A* **2006**, *74*, 032320. [CrossRef]

22. Ecker, S.; Bouchard, F.; Bulla, L.; Brandt, F.; Kohout, O.; Steinlechner, F.; Fickler, R.; Malik, M.; Guryanova, Y.; Ursin, R.; et al. Overcoming Noise in Entanglement Distribution. *Phys. Rev. X* **2019**, *9*, 041042. [CrossRef]

23. Bouchard, F.; Fickler, R.; Boyd, R.; Karimi, E. High-dimensional quantum cloning and applications to quantum hacking. *Sci. Adv.* **2017**, *3*, e1601915. [CrossRef] [PubMed]

24. Ma, H.; Qiao, Y.; Liu, H.; Shen, C. Numerical study of orbital angular momentum-entanglement in turbulence with adaptive optics system compensation. *Appl. Phys. B* **2018**, *124*, 1–9. [CrossRef]

25. Leonhard, N.D.; Shatokhin, V.N.; Buchleitner, A. Universal entanglement decay of photonic-orbital-angular-momentum qubit states in atmospheric turbulence. *Phys. Rev. A* **2015**, *91*, 012345. [CrossRef]

26. Yang, Y.; Yang, D.; Wang, J.; Zhu, Y.; Hu, Z.; Zhang, Y. Non-Kolmogorov atmospheric turbulence and orbital angular momentum of entangled states for optical communication. *Results Phys.* **2019**, *15*, 102676. [CrossRef]

27. Berry, M.V.; Balazs, N.L. Nonspreading wave packets. *Am. J. Phys.* **1979**, *47*, 264–267. [CrossRef]

28. Zhang, P.; Prakash, J.; Zhang, Z.; Mills, M.; Efremidis, N.; Christodoulides, D.; Chen, Z. Trapping and guiding microparticles with morphing autofocusing Airy beams. *Opt. Lett.* **2011**, *36*, 2883–2885. [CrossRef]

29. Broky, J.; Siviloglou, G.; Dogariu, A.; Christodoulides, D. Self-healing properties of optical Airy beams. *Opt. Express* **2008**, *16*, 12880–12891. [CrossRef]

30. Chu, X.; Zhou, G.; Chen, R.P. Analytical study of the self-healing property of Airy beams. *Phys. Rev. A* **2012**, *85*, 013815. [CrossRef]

31. Yue, P.; Hu, J.; Yi, X.; Xu, D.; Liu, Y. Effect of Airy Gaussian vortex beam array on reducing intermode crosstalk induced by atmospheric turbulence. *Opt. Express* **2019**, *27*, 37986–37998. [CrossRef]

32. Yan, X.; Liang, S.; Li, J.; Guo, L. Mitigating Vortex Splitting by Controlling the Wavefront Isophase Line Curvature of Vector Autofocusing Airy Vortex Beams in Free Space. *Photonics* **2022**, *9*, 325. [CrossRef]

33. Lib, O.; Bromberg, Y. Spatially entangled Airy photons. *Opt. Lett.* **2020**, *45*, 1399–1402. [CrossRef] [PubMed]

34. Yang, D.; Hu, Z.D.; Wang, S.; Zhu, Y. Influence of random media on orbital angular momentum quantum states of optical vortex beams. *Phys. Rev. A* **2022**, *105*, 053513. [CrossRef]

35. Gopaul, C.; Andrews, R. The effect of atmospheric turbulence on entangled orbital angular momentum states. *New J. Phys.* **2007**, *9*, 94. [CrossRef]

36. Paterson, C. Atmospheric Turbulence and Orbital Angular Momentum of Single Photons for Optical Communication. *Phys. Rev. Lett.* **2005**, *94*, 153901. [CrossRef]

37. Siviloglou, G.; Christodoulides, D. Accelerating finite energy Airy beams. *Opt. Lett.* **2007**, *32*, 979–981. [CrossRef]

38. Chu, X. Evolution of an Airy beam in turbulence. *Opt. Lett.* **2011**, *36*, 2701–2703. [CrossRef]
39. Zhang, X.; Shen, B.; Shi, Y.; Wang, X.; Zhang, L.; Wang, W.; Xu, J.; Yi, L.; Xu, Z. Generation of Intense High-Order Vortex Harmonics. *Phys. Rev. Lett.* **2014**, *114*, 173901. [CrossRef]
40. Cheng, M.; Guo, L.; Li, J.; Zhang, Y. Channel Capacity of the OAM-Based Free-Space Optical Communication Links With Bessel–Gauss Beams in Turbulent Ocean. *IEEE Photonics J.* **2016**, *8*, 1–11. [CrossRef]
41. Zhu, Y.; Zhang, Y.; Hu, Z. Spiral spectrum of Airy beams propagation through moderate-to-strong turbulence of maritime atmosphere. *Opt. Express* **2016**, *24*, 10847–10857. [CrossRef]
42. Efremidis, N.; Christodoulides, D. Abruptly autofocusing waves. *Opt. Lett.* **2010**, *35*, 4045–4047. [CrossRef] [PubMed]
43. Wang, X.; Yang, Z.; Zhao, S. Influence of oceanic turbulence on propagation of Airy vortex beam carrying orbital angular momentum. *Optik* **2018**, *176*, 49–55. [CrossRef]